

## A First Look at Cepheids in a SN Ia Host with *JWST*

WENLONG YUAN,<sup>1</sup> ADAM G. RIESS,<sup>1,2</sup> STEFANO CASERTANO,<sup>2</sup> AND LUCAS M. MACRI<sup>3</sup>

<sup>1</sup>*Department of Physics & Astronomy, Johns Hopkins University, Baltimore, MD 21218, USA*

<sup>2</sup>*Space Telescope Science Institute, 3700 San Martin Drive, Baltimore, MD 21218, USA*

<sup>3</sup>*George P. and Cynthia W. Mitchell Institute for Fundamental Physics and Astronomy,  
Department of Physics and Astronomy, Texas A&M University, College Station, TX 77843, USA*

### ABSTRACT

We report the first look at extragalactic Cepheid variables with the *James Webb Space Telescope*, obtained from a serendipitous (to this purpose) observation of NGC 1365, host of an SN Ia (SN 2012fr), a calibration path used to measure the Hubble constant. As expected, the high-resolution observations with NIRCcam through *F200W* show better source separation from line-of-sight companions than *HST* images at similar near-infrared wavelengths, the spectral region that has been used to mitigate the impact of host dust on distance measurements. Using the standard star P330E as a zero-point and PSF reference, we photometered 31 previously-known Cepheids in the *JWST* field, spanning  $1.15 < \log P < 1.75$  including 24 Cepheids in the longer period interval of  $1.35 < \log P < 1.75$ . We compared the resultant Period-Luminosity relations to that of 49 Cepheids in the full period range including 38 in the longer period range observed with WFC3/IR on *HST* and transformed to the *JWST* photometric system (*F200W*, Vega). The P-L relations measured with the two space telescopes are in good agreement, with intercepts (at  $\log P = 1$ ) of  $25.74 \pm 0.04$  and  $25.72 \pm 0.05$  for *HST* and *JWST*, respectively. Our baseline result comes from the longer period range where the Cepheids have higher signal-to-noise ratios where we find  $25.75 \pm 0.05$  and  $25.75 \pm 0.06$  mag for *HST* and *JWST*, respectively. We find good consistency between this first *JWST* measurement and *HST*, and no evidence that *HST* Cepheid photometry is “biased bright” at the  $\sim 0.2$  mag level that would be needed to mitigate the Hubble Tension, though comparisons from more SN hosts are warranted and anticipated. We expect future *JWST* observations to surpass these in quality as they will be optimized for measuring Cepheids.

### 1. INTRODUCTION

Cepheid variables have held a central role in measuring extragalactic distances for more than a century (Leavitt & Pickering 1912). They exhibit several features which make them uniquely suited for this role. Their nature is well understood as a consequence of the  $\kappa$  mechanism, which drives a periodic overshooting of hydrostatic equilibrium and produces their pulsations (Eddington 1927). Their great luminosities,  $\sim 10^5 L_\odot$ , make them visible with modern telescopes at many tens of Megaparsecs. The large amplitude of their variations uniquely identifies them and their periods standardize their luminosities to a precision of a few percent. They are ubiquitous in areas of recent star formation, including many hosts of Type Ia supernovae (which have still greater range). Lastly, hundreds of Cepheids in the Milky Way are in range of precise parallaxes from the ESA *Gaia* satellite to provide a 1% geometric calibration of their fiducial luminosity (Riess et al. 2022a; Cruz Reyes & Anderson 2022). For these reasons, Cepheids

are the primary distance indicator most often selected for measuring long-range distances and the Hubble constant (Riess et al. 2022b, hereafter, R22).

A succession of technological advancements has extended the reach, precision and accuracy of Cepheid distance estimates at tens of Megaparsecs. One of the original goals of the *Hubble* Space Telescope (*HST*) was to resolve extragalactic Cepheids, which was achieved in dozens of galaxies within  $\sim 20$  Mpc with the Wide Field Planetary Camera 2 (WFPC2) at optical wavelengths (Freedman et al. 2001; Sandage et al. 2006). *HST* instruments with greater sensitivity and higher resolution, ACS and WFC3/UVIS, extended this reach to  $\sim 50$  Mpc and a greater number of nearby SNe Ia and geometric calibrators (Macri et al. 2006; Riess et al. 2011; Hoffmann et al. 2016).

Given that Cepheids are found in regions of recent star formation, they are observed through interstellar dust with a mean reddening (in modestly-inclined spirals, R22) of  $E(V - I) \sim 0.3$  mag. Thus, their visible-

( $0.5\mu\text{m}$ ) and infrared- ( $0.8\mu\text{m}$ ) band measurements must account for a mean of  $\sim 0.7$  mag and  $\sim 0.4$  mag of extinction, respectively, to provide accurate distance measurements, which in consequence are sensitive to the uncertain nature of extragalactic reddening laws.

Wide-scale follow-up of Cepheids in the near-infrared (NIR), to mitigate dust effects, first became practical with WFC3/IR, allowing measurements at  $1.6\mu\text{m}$  and reducing the mean impact of extinction to  $\sim 0.1$  mag and the sensitivity to reddening laws (Riess et al. 2011). However, the advantage of NIR observations over optical bands came with new challenges; at these wavelengths, the resolution of *HST* is 2-3 times lower and the background (in the form of ubiquitous red giants) is an order of magnitude greater. The result is an increase in the measurement errors (after *statistical* removal of the backgrounds measured using artificial stars) which may limit the precision of distance measurements without a large number ( $>50$ ) of Cepheids in each host. While Cepheid distance measurements from either the optical or NIR are in good agreement (R22), a result most likely if both are accurate, the pursuit of a 1% measurement of the Hubble constant demands ever more stringent tests of Cepheid photometry.

The newly-launched *James Webb* Space Telescope (*JWST*) offers the twin advantages of angular resolution comparable to WFC3/UVIS at visible wavelengths and the lower impact of interstellar dust as WFC3/IR in the same observation. *JWST* observations planned for its first GO cycle have been designed to take advantage of these capabilities and reobserve Cepheids previously measured with *HST*, work which is likely to require years to collect and thoroughly analyze to fully come to fruition. However, an early observation with *JWST* of a SN Ia host previously observed by *HST* offers a serendipitous (for this endeavor) and valuable preview.

To be clear in setting expectations for future *JWST* observations, these *serendipitous* observations of the Cepheids in NGC 1365 fall short of demonstrating the full capability of the observatory for this endeavor. They are shorter in exposure time by a factor of a few than those planned for this purpose and they are obtained at nearly twice the wavelength needed to optimally resolve and reduce the contributions of nearby red giants (i.e., the background). Notably, they cover a more crowded region along a spiral arm (see Figure 1) compared to most of those observed by *HST*. Further, they provide only a single (i.e., “random”) epoch or phase in each Cepheid light curve, which adds an additional dispersion of 0.1 to 0.2 mag depending on the amplitude of the Cepheid. Lastly, the state of the *JWST* calibration data (e.g., flat fields, dark frames, bias frames, geomet-

ric distortion maps, linearity corrections) is in its first iteration and will improve with time. Nevertheless, and with these limitations in mind, these observations preview the enhanced capabilities of *JWST* over *HST* and provide meaningful, if preliminary, quantitative results.

In §2 we describe the details of the *JWST* observations for NGC 1365, as well as the data reduction and photometry procedures. We show our results in §3 and a brief discussion in §4. An appendix provides information about past *HST* observations of Cepheids in NGC 1365 for easy reference.

## 2. OBSERVATIONS, DATA REDUCTION, AND PHOTOMETRY

### 2.1. Observations & data reduction

The central region of NGC 1365 was recently observed with *JWST* NIRCам on 2022 August 13 as part of program GO-2107 (PI: Janice Lee), which aims to study the star formation activity in 19 nearby galaxies. The NGC 1365 field partially overlaps with an *HST* WFPC2 time-series field (GO-5972, PI: Jeremy Mould) where dozens of Cepheids were discovered (Silbermann et al. 1999; Hoffmann et al. 2016) and followed up in the NIR (R22). With the Cepheid locations and periods determined from those *HST* data, we have an opportunity to photometer and study these Cepheids in the new *JWST* observations. In Figure 1 we show the footprints of the *JWST* observations as well as archival *HST* observations and locations of previously-identified Cepheids. The initial WFPC2 time-series and WFC3 follow-up targeted a less crowded part of the host off the spiral arms, but the NIRCам observations targeted the center of the galaxy and primarily contain Cepheids in a small dense, crowded region. Appendix Figure A1 shows less-crowded Cepheids imaged by *HST* that are more similar to those typically studied in *HST* fields. Due to the overlap of the two observatories, we can also directly compare the images and measurements of many of the same Cepheids in the denser regions of the host.

We retrieved *JWST* observations of NGC 1365 from MAST and processed the raw data (stage 0) using the *JWST* Science Calibration Pipeline version 1.6.2. There are 25 exposures in total, with the short-wavelength channel through the *F200W* filter and the long-wavelength channel through the *F300M*, *F335M*, and *F360M* filters. In this study, we only analyzed the *F200W* data for their depth and proximity in wavelength coverage compared to the *HST F160W* band. The *F200W* data consist of eight subfields, with each one covered by approximately one short-wavelength detector. Only the two east-most subfields contain previously-



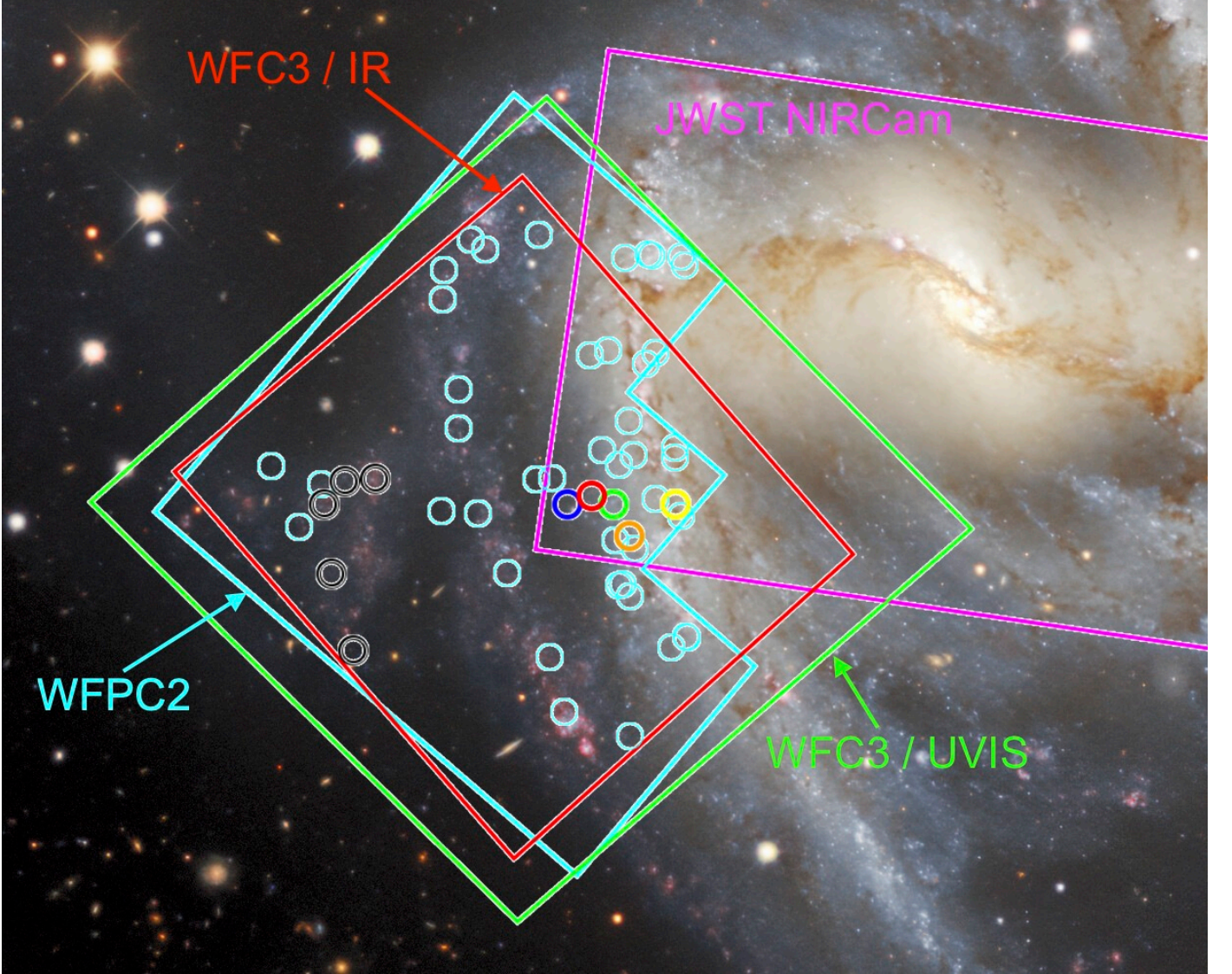


**Figure 1.** Observation footprints of NGC 1365 with *JWST* NIRCcam (magenta), *HST* WFPC2 (cyan), WFC3/UVIS (green), and WFC3/IR (red) overlaid on a color composite image from the Dark Energy Survey (DOE/FNAL/DECam/CTIO/NOIRLab/NSF/AURA). The locations of Cepheids used in this study are indicated by circles. North is up and east is to the left.

identified Cepheids; thus, we excluded the other six from the analysis. The total exposure times are 1202.52s for both analyzed subfields.

We noticed the  $1/f$  noise causing small bias shifts in the calibrated stage 2 data products (see §2 of [Merlin et al. 2022](#)). We corrected them by subtracting the median value of each row and then each column before the *JWST* pipeline stage 3 process. Similar to [Merlin et al. \(2022\)](#), we masked all sources when computing the median values for row and column subtractions.

We used the WCS in the images to locate the Cepheids based on their *HST* positions. We identified a global shift of  $\sim 0''.5$  between the *HST* and *JWST* positions and accounted for this to register the images. After this

global shift we found point sources at the expected positions of the Cepheids to a precision of less than a NIRCcam pixel ( $0''.031$ ; see Figure 2). The *HST* NIR observations in these spiral arms are under-sampled (even after drizzling to  $0''.08$ /pixel resolution) and lack the inherent resolution of *JWST* (despite the greater wavelength of those observations).

While the Cepheids were easily apparent in the deeper and higher-resolution images in *F200W*, they were hard to discern in the accompanying observations at longer-wavelengths and through medium-width bands due to their much shorter exposure times, lower angular resolution and lower throughput of these filters. As a result we only analyzed the *F200W* images.

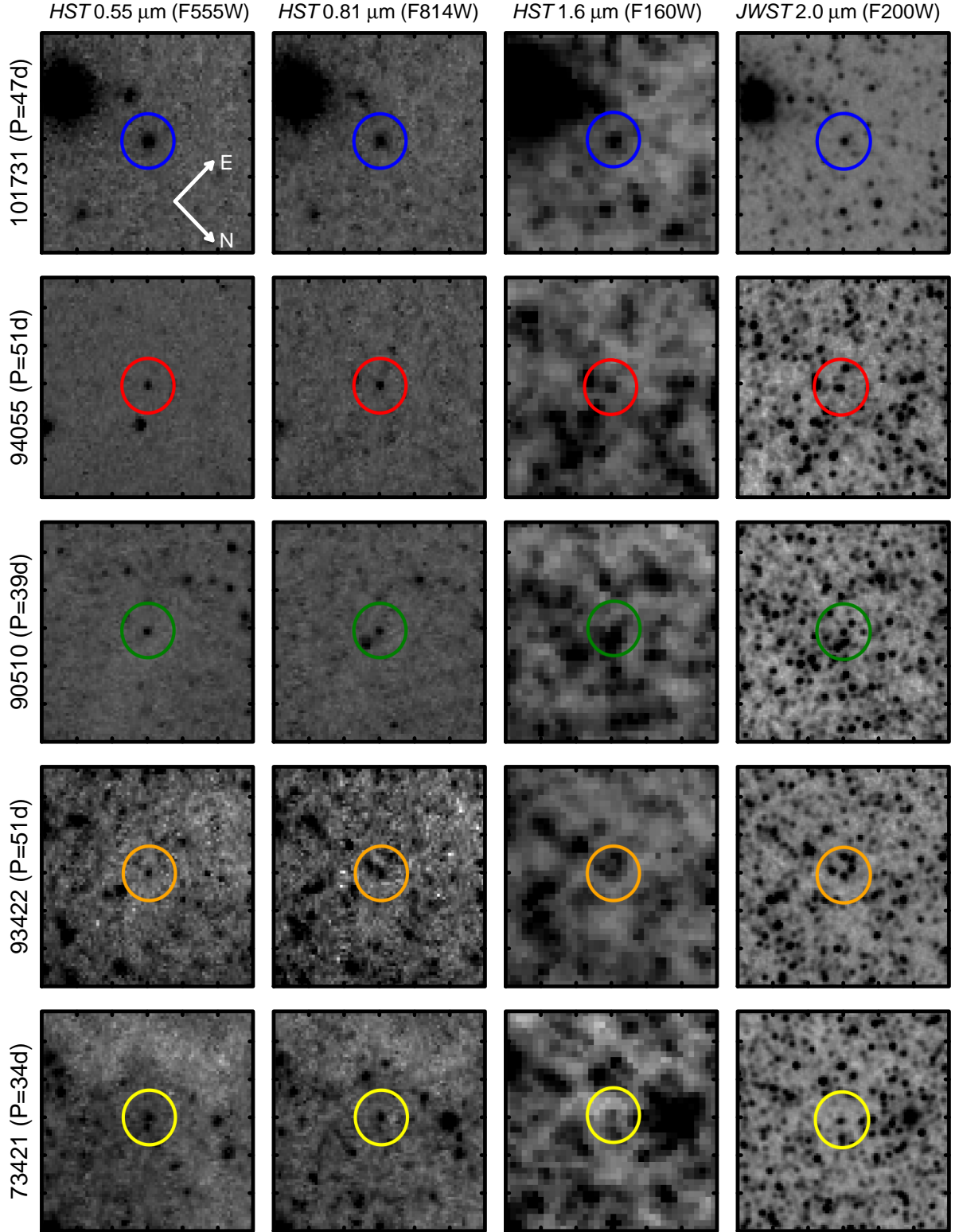


**Figure 2.** Image cuts of 5 example Cepheids analyzed in this study. Their locations are indicated by the corresponding colors in Figure 1. The circles cover a radius of  $0''.375$  while the image cuts display  $3''$  in a side. From left to right, each row shows one (same) Cepheid in *HST* *F555W*, *F814W*, *F160W*, and *JWST* *F200W*, where the exposure times are 1410s, 1770s, 3618s, and 1203s, respectively. The orientation of the image cuts is indicated by the white compass in the top-left panel.



## 2.2. Photometry

We performed point-spread function (PSF) photometry using a crowded-field photometry package based on DAOPHOT/ALLSTAR [Stetson \(1987, 1994\)](#). We constructed an empirical model of the PSF using *F200W* observations of the standard star P330E (taken on 2022 Aug 29, obs. ID=jw01538o155t002) obtained in a 160-pixel subarray (using a minimal exposure time to keep the star below saturation) which included two dithers placed on each of the B-module chips.

We chose not to use the pipeline calibration to obtain the image zeropoints as they have been found to have limited accuracy (at the time of this writing) including chip-to-chip offsets (and possible time-dependence between the early life of the mission and the present, [Brammer 2022](#); [Boyer et al. 2022](#); [Nardiello et al. 2022](#)). To produce reliable zeropoints for the observation of NGC 1365 we used the above observations of P330E obtained and combined for each B-module chip separately to directly calibrate the Cepheids observed in that chip. We assigned each image of P330E a reference Vega magnitude of 11.42 mag ([Rieke et al. 2022](#)). An important advantage of using the Aug 29, 2022 observations of P330E to set the zeropoints for the images of NGC 1365 is that they were obtained only 2 weeks after the observation of NGC 1365, an interval during which *JWST*’s wave front monitoring has shown it to be relatively stable with modeled photometric variations over the interval of  $< 0.01$  mag (M. Perrin, 2022 private communication). (We did not make use of aperture photometry for the Cepheids due to the inability to separate nearby sources as expected from inspection of Figure 2.)

To avoid a flux bias from the determination of Cepheid positions in *HST* NIR images, it is necessary to fix their locations using the uncrowded optical images (i.e., “forced photometry”, [Riess et al. 2009](#)). The algorithm fits the PSF of the Cepheids at their known, fixed positions, subtracts them from the images, identifies additional, unresolved sources down to a fixed threshold, and then simultaneously optimizes the fit to the non-Cepheids (parameters are  $x$ ,  $y$  and flux) and Cepheids (parameter is flux) to determine the latter’s flux. We then add “artificial stars” at the same brightness as the Cepheid (based on the period and iterative fit of the Period-Luminosity relation), and remeasure these using the same procedure to account for the mean background of unresolved sources near the position of the Cepheid (i.e., a statistical crowding correction) and to measure the uncertainty in the Cepheid magnitude. We also compared our results to the level 3, full-calibrated

images produced by the STScI pipeline and found that the photometry was consistent between the versions of the images.

## 3. RESULTS

Fixing the slope of the Period-Luminosity relation to the global value of  $-3.30$  determined from the mean of thousands of Cepheids in the MW, LMC, SMC, M31, NGC 4258 and SN Ia hosts in the NIR (R22), we measured the intercepts at  $\log P = 1$ .

For our “baseline”, we limited the comparison to a period range of  $1.35 < \log P < 1.75$  where the Cepheids as measured from both telescopes have strong signal-to-noise ratios. Below this range the SNR at *F160W* = 24.5 (Vega) drops to  $< 10$  and above this range Cepheid periods in NGC 1365 are not expected to be accurate because the original time-series used to find the Cepheids in NGC 1365 spanned only 48 days ( $\log P = 1.68$ ), so that a full cycle would not have been seen. The *JWST* and *HST* Cepheid Period-Luminosity relations are shown in Figure 3.

For *JWST* with PSF fitting (referenced to P330E) and with 24 Cepheids we find an intercept of  $25.75 \pm 0.06$  (SD=0.36 mag). In Table 2 we provide intercepts for broader ranges of periods and with and without  $\sigma$  clipping.

To directly compare the *HST* and *JWST* Period-Luminosity relations observed at different, though adjacent, bandpasses, it is necessary to account for their different wavelength responses. Due to the simple spectral energy distributions of stars, particularly on the Rayleigh-Jeans tail in the NIR, it is relatively straightforward to estimate this difference, which is the color *F160W*–*F200W*, from another measured color such as *F555W*–*F814W*. To do this rigorously we used the PARSEC isochrones ([Bressan et al. 2012](#)) for stellar atmospheres which are provided as calculated for the *HST* and *JWST* bandpasses (using version CMD v3.6, <http://stev.oapd.inaf.it/cgi-bin/cmd>). We limited these to a range appropriate for Cepheids: ages of 10 to 100 Myr,  $T_{\text{eff}}$  of 4000 to 7000 degrees, initial masses  $> 2M_{\odot}$ , and  $\log g < 2$ . These stars have a tight locus in the color-color plane of WFC3/UVIS for *F555W*–*F814W* vs *F160W* (*HST*)–*F200W* (*JWST*). We fit a second-order polynomial to the color-color relation, finding

$$F160W - F200W = 0.007 + 0.053(F555W - F814W) + 0.077(F555W - F814W)^2$$

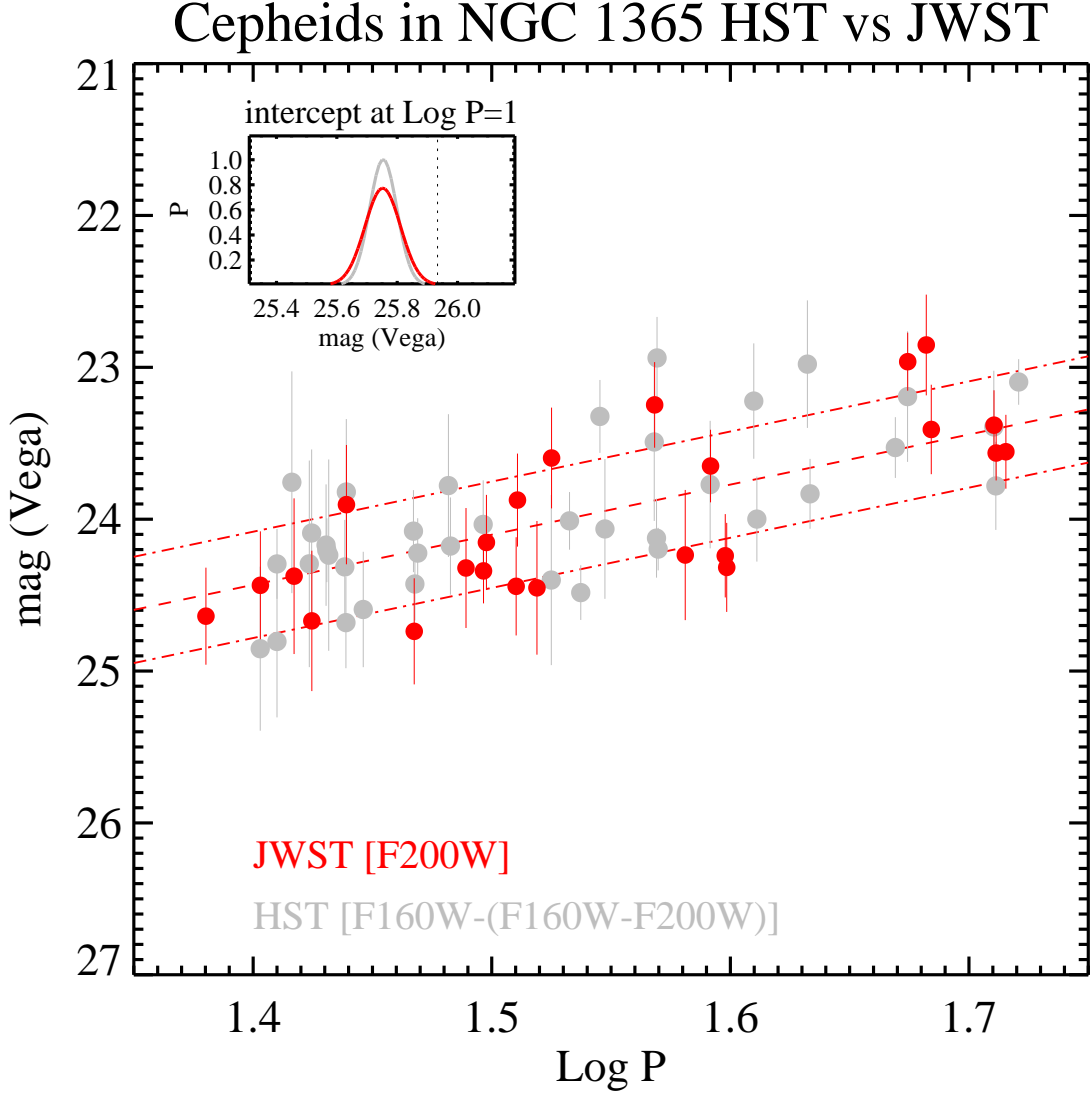


**Figure 3.** Near-infrared Period-Luminosity relations for Cepheids in the range  $1.35 < \log P < 1.75$  (baseline results) measured with *HST* and *JWST*. The *JWST* sample (red) includes 24 Cepheids observed in *F200W* ( $2\mu\text{m}$ ). The *HST* sample includes 38 Cepheids from R22 with *F160W* magnitudes transformed to *F200W* using a color transformation based on their measured  $V - I$  colors and  $F160W - F200W$ . The inset shows the intercepts of the relations at  $\log P = 1$ . The solid red curve uses the *JWST* PSF photometry calibrated to P330E.

**Table 1.** *JWST F200W* Cepheid Photometry

ID	$P$	$F200W^a$	$\sigma^b$	R.A. <sup>c</sup>	Decl.	subfield
	[days]	[mag]		[deg] (J2000.0)		
97917	24.00	24.64	0.32	53.433156	-36.158061	south
60205	25.30	24.44	0.36	53.435680	-36.144208	south
25668	26.13	24.38	0.51	53.432499	-36.136873	north
74699	26.58	24.67	0.46	53.427052	-36.156193	south
40364	27.48	23.90	0.39	53.429580	-36.143996	south
65664	29.34	24.74	0.35	53.431935	-36.149101	south
53380	30.85	24.32	0.40	53.433946	-36.143847	south
100027	31.37	24.34	0.21	53.439120	-36.153423	south
79315	31.46	24.15	0.31	53.432884	-36.152400	south
80300	32.38	24.44	0.32	53.434414	-36.151327	south
94995	32.42	23.87	0.31	53.431335	-36.158716	south
45761	33.03	24.45	0.44	53.430433	-36.144804	south
73421	33.50	23.60	0.33	53.427504	-36.155372	south
61628	37.01	23.25	0.28	53.427674	-36.151793	south
17203	38.12	24.24	0.43	53.430027	-36.136683	north
90510	39.06	23.65	0.24	53.433311	-36.155466	south
77265	39.61	24.24	0.27	53.429382	-36.154908	south
58983	39.67	24.32	0.29	53.427627	-36.151066	south
101731	47.24	22.96	0.19	53.437542	-36.155483	south
8616	48.09	22.85	0.33	53.427309	-36.136727	north
9712	48.33	23.41	0.29	53.426932	-36.137379	north
93422	51.34	23.38	0.23	53.431778	-36.157790	south
94055	51.45	23.56	0.18	53.435355	-36.154809	south
17544	51.94	23.56	0.24	53.430280	-36.136566	north

NOTE— *a*: These are Vega mag referenced to P330E = 11.42 in *F200W*. *b*: The errors are derived from artificial stars and also include a random phase error in quadrature of 0.15 mag. *c*: Positions are referenced to the WCS of *JWST* images processed using *JWST* pipeline v1.6.2.

**Table 2.** *HST* and *JWST* Intercepts at  $\log P = 1$  (slope=−3.30) for NIR Cepheids in NGC 1365

Sample	$N$ Cepheids	Period range	$F200W$ Intercept <sup>a</sup>
<b><i>HST</i> WFC3/IR field, baseline</b>	<b>38</b>	<b><math>1.35 &lt; \log P &lt; 1.75</math></b>	<b><math>25.754 \pm 0.045</math></b>
<i>HST</i> WFC3/IR field, extended	49	$1.15 < \log P < 1.75$	$25.736 \pm 0.043$
<i>HST</i> WFC3/IR field, SH0ES R22 <sup>b</sup>	46	$15.0 < P < 50.0$	$25.750 \pm 0.045$
<b><i>JWST</i> NIRCcam field, baseline, PSF</b>	<b>24</b>	<b><math>1.35 &lt; \log P &lt; 1.75</math></b>	<b><math>25.752 \pm 0.059</math></b>
<i>JWST</i> NIRCcam field, extended, PSF	31	$1.15 < \log P < 1.75$	$25.718 \pm 0.055$

NOTE— *a*: Results from *HST* measured in *F160W* and converted to *F200W* using  $F160W - F200W = 0.007 + 0.053(F555W - F814W) + 0.077(F555W - F814W)^2$ . *b*: Same period range and sample used in R22.

The dispersion of the synthetic values around this approximation is 0.007 mag. The mean Cepheid color of the sample is  $F555W - F814W = 1.08$  mag (sample SD=0.22 mag) where the relation gives  $F160W - F200W = 0.15$  mag (sample SD=0.05 mag), however we computed the individual values for each Cepheid, as given in the Appendix. We subtract the individual  $F160W - F200W$  colors predicted from the optical colors from the measured *HST*  $F160W$  to provide a direct comparison to *JWST*  $F200W$  as shown in Figure 3.

The baseline measurements of the *HST* intercepts use the  $F160W$  magnitudes as given in R22, the  $F160W - F200W$  colors as given in the Appendix, and include 38 Cepheids in this period range. To increase the sample for the purpose of this *HST* to *JWST* comparison, we added 3 Cepheids with  $P = 51, 51$ , and 52 days found by Hoffmann et al. (2016) and only slightly above the  $P < 50$  day limit used by R22 but still well below the  $1.2\times$  time-span of the observations necessary to be reliable. We find an intercept for *HST* at  $\log P = 1$  of  $25.75 \pm 0.05$  mag and provide intercepts with other period ranges in Table 2.

The inset in Figure 3 compares the intercepts. The agreement between the *HST* and *JWST* intercepts is very good, below  $1\sigma$  in their difference. The same mean difference is seen when comparing only identical Cepheids though the number of Cepheids measured by both is far smaller and thus the comparison is less significant. The dispersion around the Period-Luminosity relation as shown in Figure 3 is comparable between *HST* and *JWST* and is likely to be smaller for optimal *JWST* observations with multiple epochs, better image calibration and in less crowded regions more typically observed with *HST*.

To a  $\sim 0.05$  mag level of preliminary accuracy based on still limited characterization of *JWST* and for this case we can conclude that past *HST* NIR measurements do not appear biased, let alone “biased bright” at the  $\sim 0.2$  mag level (i.e., by the systematics of past photometry measurements or by previously unresolved companions) as could mitigate the “Hubble Tension” in R22 (and then only if such a bias was not also similarly present in *HST* photometry of Cepheids in the geometric anchor, NGC 4258).

#### 4. DISCUSSION

The *JWST* images and measurements of Cepheids in NGC 1365 and in comparison to those from *HST* bode well for the quality of such future measurements. We reiterate that these observations were not optimized for observing Cepheids and are far from the best that *JWST* can do. Optimal observations would be longer

in exposure time, cover multiple passbands to the necessary depth, include shorter wavelengths for better resolution, include multiple epochs to reduce the random phase noise, have higher signal-to-noise calibration frames (flats, darks, bias frames, chip offsets, geometric distortion for locating Cepheids, etc) available and better cover the regions where past *HST* programs have found Cepheids and measured their periods.

We also note that it is too early in the life of *JWST* and NIRCcam to identify and calibrate subtle photometric effects. There is one such effect we are aware of, the count-rate non-linearity (CRNL), which makes faint objects appear fainter, though the scale of this effect has been diminishing with improvements in NIR detector manufacturing and testing used to select the best chips. Because the level of CRNL has not yet been measured in space for NIRCcam, we did not correct either the NIRCcam or the WFC3/IR Cepheid photometry for this effect, so to first approximation we might expect that CRNL cancels in the comparisons provided here. For WFC3/IR, CRNL makes the Cepheids in NGC 1365  $\sim 0.03$  mag faint relative to the flux level of standard stars (Riess et al. 2009). If the CRNL of NIRCcam is  $\sim$  half the level of WFC3/IR (our guess), the error in the comparison will be  $\sim 0.015$  mag, negligible at the precision of *this* study, but important to calibrate for future, larger samples. The single-epoch sampling of this *JWST* observation introduces a statistical bias of  $\sim 0.005$  mag in the Cepheid Period-Luminosity relation compared to the typical flux-averaged (multi-epoch) observations. This bias is again negligible for the precision of this study.

Nevertheless, the quantitative comparison of the first *JWST* Cepheid Period-Luminosity intercepts presented here is promising, and already significant as a check on past *HST* measurements. We expect that the calibration of this observatory will only improve and mature, leading to future observations that should provide ever more definitive investigations.

We are indebted to all of those who spent years and even decades bringing *JWST* to fruition. We are grateful to the proposers of GO-2107 (PI: Janice Lee) for making their program non-proprietary, enabling the community to undertake assorted investigations from this data including this study. This research made use of the NASA’s Astrophysics Data System.



## REFERENCES

- Boyer, M. L., Anderson, J., Gennaro, M., et al. 2022, arXiv e-prints, arXiv:2209.03348. <https://arxiv.org/abs/2209.03348>
- Brammer, G. 2022, grizli, 1.5.0, doi: [10.5281/zenodo.5012699](https://doi.org/10.5281/zenodo.5012699)
- Bressan, A., Marigo, P., Girardi, L., et al. 2012, MNRAS, 427, 127, doi: [10.1111/j.1365-2966.2012.21948.x](https://doi.org/10.1111/j.1365-2966.2012.21948.x)
- Cruz Reyes, M., & Anderson, R. I. 2022, arXiv e-prints, arXiv:2208.09403. <https://arxiv.org/abs/2208.09403>
- Eddington, A. S. 1927, MNRAS, 87, 539, doi: [10.1093/mnras/87.7.539](https://doi.org/10.1093/mnras/87.7.539)
- Freedman, W. L., Madore, B. F., Gibson, B. K., et al. 2001, ApJ, 553, 47, doi: [10.1086/320638](https://doi.org/10.1086/320638)
- Hoffmann, S. L., Macri, L. M., Riess, A. G., et al. 2016, ApJ, 830, 10, doi: [10.3847/0004-637X/830/1/10](https://doi.org/10.3847/0004-637X/830/1/10)
- Leavitt, H. S., & Pickering, E. C. 1912, Harvard College Observatory Circular, 173, 1
- Macri, L. M., Stanek, K. Z., Bersier, D., Greenhill, L. J., & Reid, M. J. 2006, ApJ, 652, 1133, doi: [10.1086/508530](https://doi.org/10.1086/508530)
- Merlin, E., Bonchi, A., Paris, D., et al. 2022, arXiv e-prints, arXiv:2207.11701. <https://arxiv.org/abs/2207.11701>
- Nardiello, D., Bedin, L. R., Burgasser, A., et al. 2022, arXiv e-prints, arXiv:2209.06547. <https://arxiv.org/abs/2209.06547>
- Rieke, G. H., Su, K., Sloan, G. C., & Schlawin, E. 2022, AJ, 163, 45, doi: [10.3847/1538-3881/ac3b5d](https://doi.org/10.3847/1538-3881/ac3b5d)
- Riess, A. G., Macri, L., Casertano, S., et al. 2009, ApJ, 699, 539, doi: [10.1088/0004-637X/699/1/539](https://doi.org/10.1088/0004-637X/699/1/539)
- . 2011, ApJ, 730, 119, doi: [10.1088/0004-637X/730/2/119](https://doi.org/10.1088/0004-637X/730/2/119)
- Riess, A. G., Breuval, L., Yuan, W., et al. 2022a, arXiv e-prints, arXiv:2208.01045. <https://arxiv.org/abs/2208.01045>
- Riess, A. G., Yuan, W., Macri, L. M., et al. 2022b, ApJL, 934, L7, doi: [10.3847/2041-8213/ac5c5b](https://doi.org/10.3847/2041-8213/ac5c5b)
- Sandage, A., Tammann, G. A., Saha, A., et al. 2006, ApJ, 653, 843, doi: [10.1086/508853](https://doi.org/10.1086/508853)
- Silbermann, N. A., Harding, P., Ferrarese, L., et al. 1999, ApJ, 515, 1, doi: [10.1086/307002](https://doi.org/10.1086/307002)
- Stetson, P. B. 1987, PASP, 99, 191, doi: [10.1086/131977](https://doi.org/10.1086/131977)
- . 1994, PASP, 106, 250, doi: [10.1086/133378](https://doi.org/10.1086/133378)

## APPENDIX

A. CEPHEID MEASUREMENTS FROM *HST***Table A1.** *HST F160W* Cepheid Photometry

ID	<i>P</i>	<i>F160W</i>	$\sigma$	<i>F555W</i> – <i>F814W</i>	<i>F160W</i> – <i>F200W</i>	R.A. <sup><i>a</i></sup>	Decl.
	[days]			[mag]		[deg] (J2000.0)	
60205	25.16	25.03	0.54	1.18	0.18	53.435572	-36.144146
136735	25.57	24.41	0.23	0.89	0.12	53.465135	-36.152743
43927	25.57	24.98	0.50	1.17	0.17	53.440450	-36.135135
101154	25.94	23.89	0.73	0.98	0.13	53.426225	-36.165263
106082	26.38	24.40	0.68	0.84	0.11	53.432670	-36.161386
74699	26.44	24.28	0.55	1.23	0.19	53.426941	-36.156136
63449	26.81	24.39	0.40	1.35	0.22	53.445400	-36.136227
138773	26.83	24.35	0.21	1.04	0.15	53.462525	-36.157297
101112	26.88	24.37	0.63	0.98	0.13	53.426292	-36.165183
120972	27.30	24.46	0.31	1.04	0.15	53.443078	-36.160625
126914	27.33	24.78	0.30	0.80	0.10	53.455397	-36.153646
40364	27.34	23.94	0.48	0.91	0.12	53.429471	-36.143937
65336	27.79	24.71	0.38	0.89	0.12	53.446800	-36.135500
124631	29.17	24.22	0.27	1.02	0.14	53.438970	-36.166817
130859	29.21	24.56	0.24	0.98	0.13	53.458170	-36.153817
133465	29.29	24.44	0.23	1.34	0.22	53.460423	-36.154001
105797	30.17	23.98	0.47	1.28	0.20	53.431618	-36.162206
106470	30.23	24.30	0.32	0.93	0.12	53.427648	-36.166054
100027	31.20	24.11	0.29	0.66	0.08	53.439011	-36.153369
73421	33.32	24.52	0.56	0.91	0.12	53.427399	-36.155314
122163	33.91	24.20	0.19	1.23	0.19	53.449210	-36.155957
139368	34.28	24.64	0.18	1.09	0.16	53.459369	-36.160824
87703	34.92	23.51	0.24	1.22	0.19	53.449343	-36.140061
117850	35.09	24.21	0.46	1.04	0.15	53.445830	-36.156138
61628	36.80	23.79	0.52	1.63	0.30	53.427562	-36.151741
103387	36.88	24.25	0.26	0.94	0.12	53.447790	-36.146777
80315	36.90	23.12	0.27	1.20	0.18	53.449213	-36.137887
142648	36.94	24.32	0.14	0.93	0.12	53.457318	-36.166545
90510	38.84	23.92	0.42	1.05	0.15	53.433201	-36.155411
128912	40.51	23.39	0.38	1.14	0.17	53.437587	-36.170953
103704	40.63	24.24	0.28	1.43	0.24	53.440403	-36.153516
104907	42.66	23.14	0.42	1.11	0.16	53.432245	-36.161310
123489	42.77	23.96	0.23	0.95	0.13	53.431458	-36.172785
109560	46.44	23.80	0.20	1.54	0.27	53.447707	-36.149730
101731	46.99	23.31	0.43	0.90	0.12	53.437427	-36.155425
93422	51.07	23.65	0.37	1.49	0.26	53.431666	-36.157737
94055	51.17	24.00	0.29	1.35	0.22	53.435250	-36.154750
134975	52.31	23.21	0.15	0.88	0.11	53.460099	-36.155567

NOTE— *a*: Positions are referenced to the WCS of *HST F160W* images processed using **AstroDrizzle v2.2.6**.

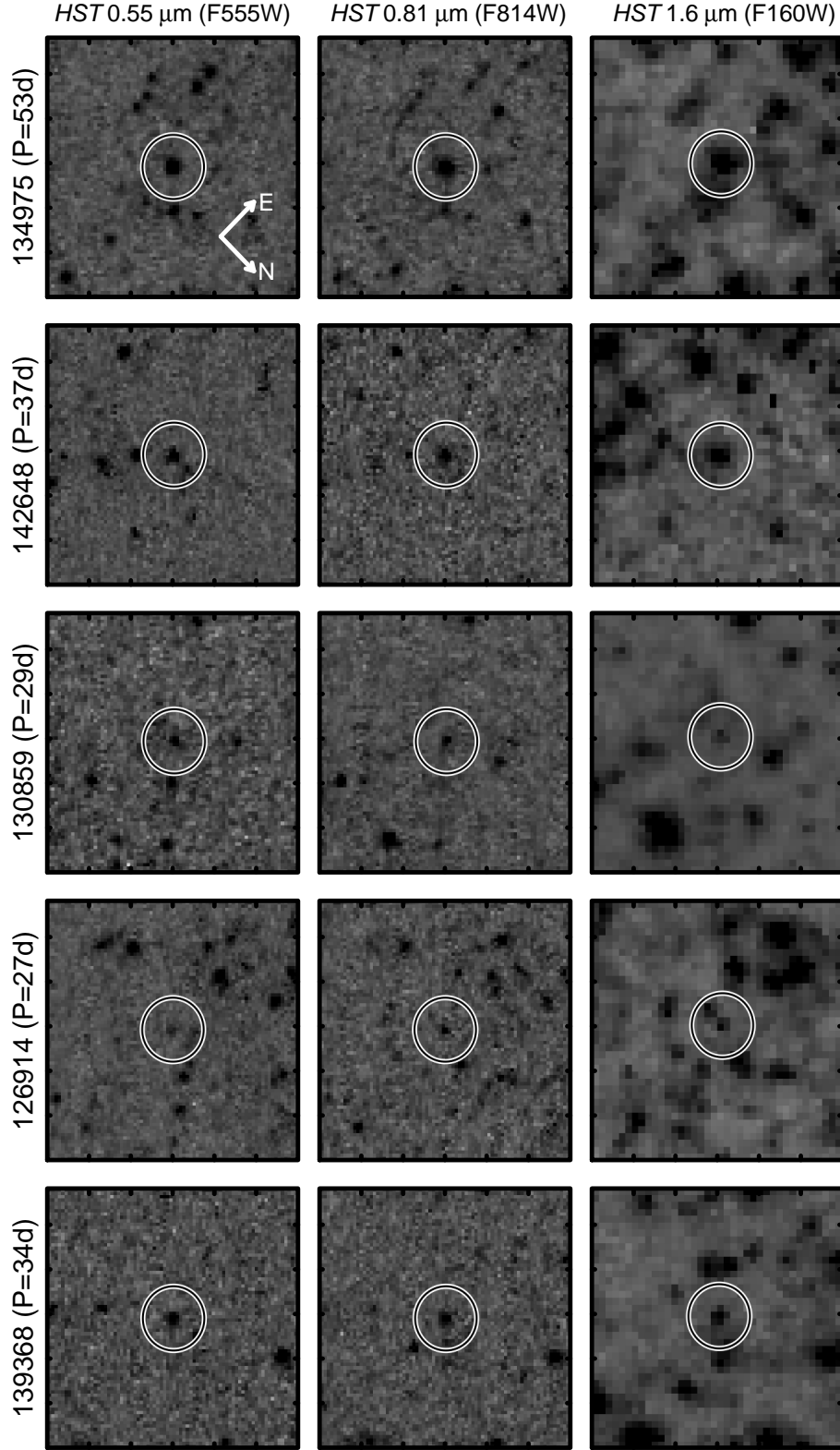


**Figure A1.** Same as Figure 2 but for 5 examples in the more typical, lower-density *HST F160W* field, where *JWST* observations are not available. See Figure 1 for location.